

Award Accounts

The Chemical Society of Japan Award for Young Chemists for 2004

Photo-Control of Magnetization by Photochromic Compounds

Yasuaki Einaga

Department of Chemistry, Faculty of Science and Technology, Keio University, 3-14-1 Hiyoshi, Kohoku-ku, Yokohama 223-8522

Received August 1, 2005; E-mail: einaga@chem.keio.ac.jp

The development of new magnetic materials in which magnetic properties are combined with optical properties has been extensively studied. So far, several photo-responsive molecular solids have been reported. However, the strategies that are necessary to achieve photoinduced switching in a solid state are yet to be clarified. Here, I have focused on composite materials as a novel strategy for realizing such photo-functional magnetic systems. These include the incorporation of organic photochromes into magnetic systems, e.g., photo-controllable magnetic vesicles and LB films containing Prussian blue or iron oxide nanoparticles and azobenzene.

Optically-switchable magnetic materials are becoming increasingly important in the field of high density information storage media, because the photon mode allows us to access a variety of different types of materials with high speed and superior resolution.[1–3] In particular, the design of molecular compounds that exhibit photoinduced magnetization behavior has attracted great attention.[4,5] In fact, several molecular photomagnetic materials were developed. They include, for example, cyanide-bridged complexes such as Prussian blue analogues,[6–8] and crystalline metal-assembled complexes.[9] Although reversible photo-control of magnetic properties or electronic states including spin states were realized in these compounds, most of the interesting phenomena were observed only at low temperature. Furthermore, the number of the optically switchable molecular solids reported has been quite small. This is because the strategies that are necessary to achieve photoinduced switching in a solid state are yet to be clarified.

On the other hand, the use of organized organic assemblies to direct the formation of mesoscopic inorganic structures under mild conditions is of topical interest.[10–16] In particular, attempts to intercalate inorganic materials into functional organic molecules offer many possibilities for developing novel functional materials whose physicochemical properties are superior to those of conventional materials. Likewise, the design and synthesis of functional materials with nanometer dimensions (mesoscopic materials) are also subjects of intense current research. Although several studies have been devoted to the synthesis of nanometer-sized compound semiconductors, relatively little work exists for magnetic materials of similar dimensions.

Here, I will describe several examples of the photo-switching magnetic systems designed by a novel strategy, i.e., preparing composite magnetic materials containing photochromic compounds. Up to now, researchers have found that the photo-switching *at room temperature* was also possible by designing photochromic compound-modified magnetic nanoparticles. This article shows that this strategy is useful for the development of the photo-functional magnetic materials.

1. Photo-Controllable Magnetic Vesicles Containing Prussian Blue and Azobenzene—First Example of the Photochromic Magnetic Materials—[17]

Firstly, we introduce the first successful example of preparation of the photochromic magnetic materials. A commercially available double-chain ammonium amphiphile, didodecyldimethylammonium bromide ($[CH_3(CH_2)_{11}]_2(CH_3)_2N^+Br^-$), which forms vesicle structure in aqueous solution by sonication, and an azobenzene-containing amphiphile ($C_{12}AzoC_5N^+Br^-$), which was synthesized according to a reported procedure, were mixed with an aqueous solution of poly(vinyl alcohol) (PVA). The photochromic vesicle films were prepared by casting the above solution on a clean glass plate at room temperature (Fig. 1). In order to intercalate Prussian blue, a molecule-based magnetic material, we first dipped the cast film in aqueous $K_3[Fe(CN)_6]$ solution to exchange the hexacyanoferrate(III) anion with the bromide ion. After washing with deionized H_2O, the compound was dipped in aqueous $FeCl_2$ solution (Fig. 2).

A scanning electron micrograph (SEM) image of the composite film indicates the presence of ring-like and spheroidal objects of heterogeneous diameters (diameter 1000–5000 Å). This image is similar to that for vesicles formed from $[CH_3(CH_2)_{11}]_2(CH_3)_2N^+Br^-$ observed in a cast film without PVA. Photo-isomerization of azo moiety in the composite film was monitored by UV–vis absorption spectroscopy (Fig. 3). At room temperature, UV light illumination of the *trans* isomer converted it to the *cis* isomer. The peak at around 360 nm decreased, while new peaks appeared at 450 and 320 nm. The

Published on the web March 8, 2006; DOI 10.1246/bcsj.79.361

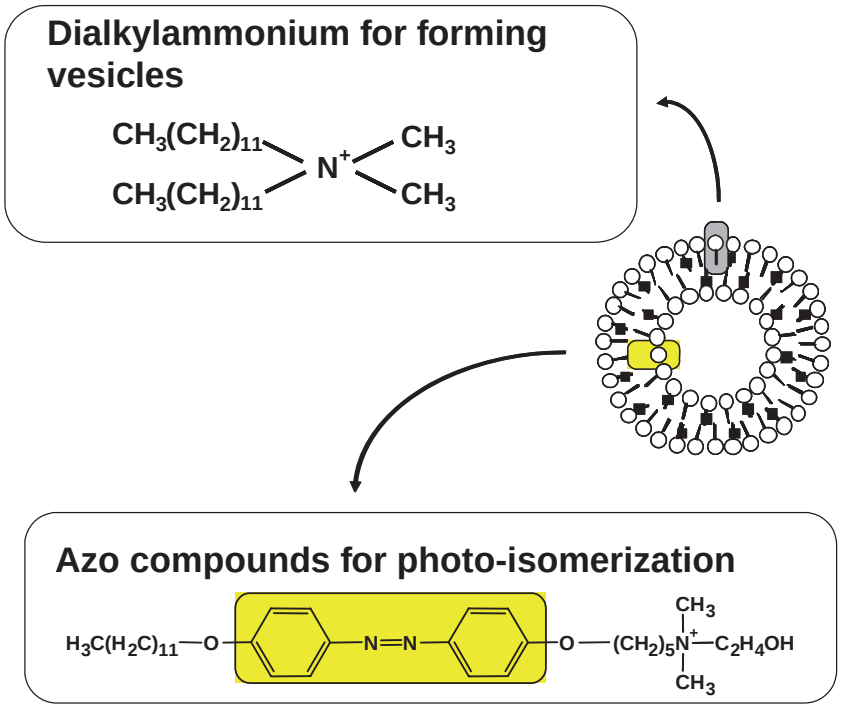

Fig. 1. Design of photo-responsive magnetic vesicles containing Prussian blue and azobenzene.

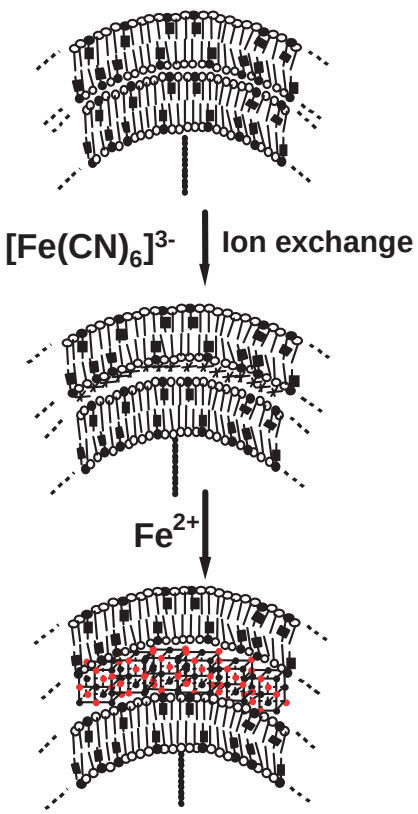

Fig. 2. Schematic illustration of the stepwise synthesis of Prussian blue in vesicles.

450 and 320 nm peaks are ascribed to the n–π^* and π–π^* transitions of the *cis* isomer, respectively. After subsequent illumination with visible light, the reverse process, i.e., the *cis*-to-*trans* isomerization proceeded completely. Therefore, the spectra obtained before and after the complete UV light illumination—visible light illumination cycle were identical. At 12 K, however, very little *trans*-to-*cis* photo-isomerization was observed even after UV light illumination for much longer times. This is because the photo-isomerization of azobenzene derivatives, particularly the *trans*-to-*cis* isomerization reaction, is accompanied by an increase in molecular volume. In fact, it is known that the solid-state reaction is greatly inhibited due to close packing of the chromophores. In contrast, by preparing the *cis* form of the film initially by UV light illumination at room temperature and then cooling it down to 12 K in a cryostat, we were able to achieve essentially complete photo-isomerization from *cis* to *trans* (conversion efficiency ca. 100%) even at low temperature. This is because the initial *cis* state, which occupies a larger geometric volume than the *trans* state, requires no additional space for the photo-isomerization. Moreover, when the isomerized *trans* form was then illuminated with UV light at 12 K, the *trans*-to-*cis* photo-isomerization proceeded to a significant degree, with a conversion efficiency of ca. 60%. The overall *trans*–*cis* isomerization cycle was then repeated several times (100% *trans* to 60% *cis*) by means of alternating illumination with visible and UV light.

Incorporation of $[Fe(CN)_6]^{3-}$ in the film was supported by ^{57}Fe Mössbauer spectroscopy. The formation of the Fe–CN–Fe framework was accomplished by immersing the film in an aqueous solution of $FeCl_2$. Figure 4 shows a SEM image of the resulting composite film. The relative amount of Fe in the film was measured using energy-dispersive X-ray spectrometry (EDX) along the line indicated in Fig. 4. This analysis suggests that the intercalated Prussian blue exists inside the vesicles, not outside. The UV absorption and Mössbauer spectra also suggest the existence of Prussian blue inside the vesicles. The absorption spectrum of the film revealed a broad peak centered at 726 nm, which is related to the intermetal

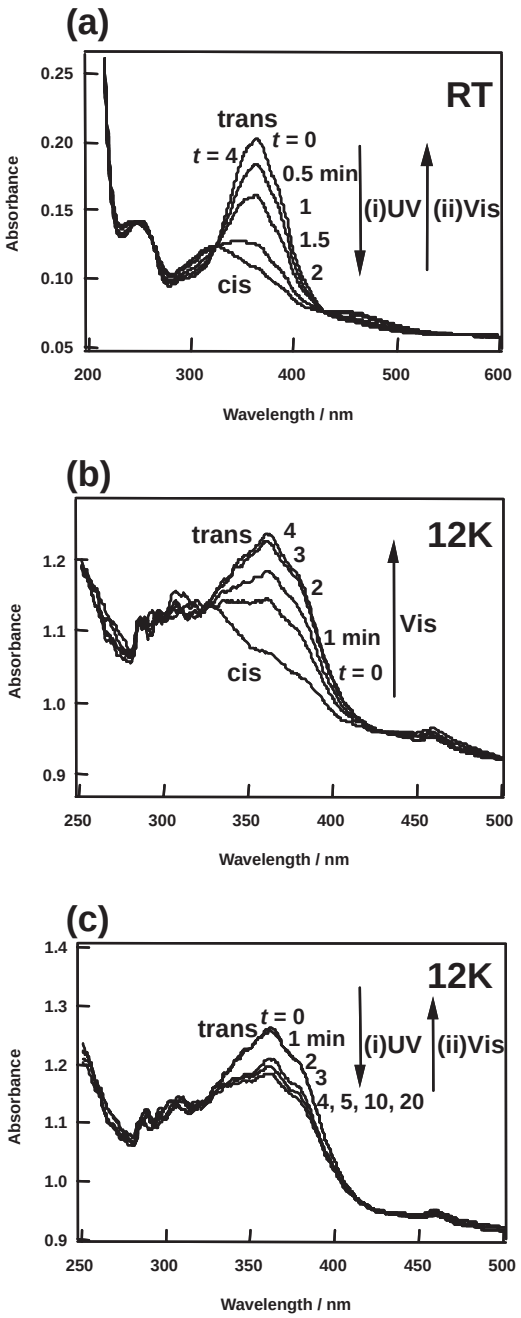

Fig. 3. Changes in the optical absorption spectra for the photo-responsive Prussian blue vesicles due to photo-isomerization. (a) At room temperature, the initial *trans* state was first illuminated with UV light for 2 min. Then, the isomerized *cis* state was illuminated with visible light for 2 min. The spectrum at time $t = 4$ min (after 2 min UV light illumination followed by 2 min visible light illumination) was identical to that at time $t = 0$ (before illumination). (b) At 12 K, the initial *cis* state was prepared by illuminating the *trans* film at room temperature, followed by cooling the film to 12 K. Then, the *cis* film was illuminated with visible light for 4 min. (c) Also at 12 K, further illumination, with UV light, of the *trans* film obtained by the process described in (b). Subsequently, *trans–cis* photoisomerization cycles were repeated by alternate illumination with UV and visible light.

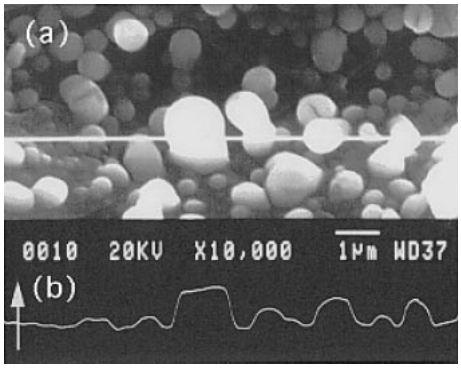

Fig. 4. (a) SEM image of the composite vesicles. (b) EDX analysis along the line indicated in part (a), showing the relative intensity for Fe along the line (arrow indicates increasing intensity).

charge-transfer band from Fe^{II} to Fe^{III}. This absorption maximum, λ_{max}, is red-shifted by ca. 26 nm from that of bulk Prussian blue.[18] This suggests that the Fe^{III} ion at the surface of the complex is coordinated by anionic hexacyanoferrate(II) ion to a lesser extent compared to hexacoordinated Fe^{III} in the bulk. In addition, it is likely that the surface of the μ-cyanide complex is in contact with the cationic bilayer surface. The existing electrostatic field will therefore lower the Coulombic energy necessary for transferring an electron from hexacyanoferrate(II) ion to the surface Fe^{III} species, thus resulting in the red-shifted absorption spectrum.[19]

The field-cooled magnetization curve at an external magnetic field of 5 G for the *cis* form of the film exhibits ferromagnetic properties with a critical temperature (T_c) of 4.2 K. This T_c value is almost identical to that of bulk Prussian blue (Fig. 5 (top)).[20] We observed the following influence of light illumination on the magnetic properties of the film. The *cis* state of the film, prepared by the UV light illumination of the *trans* film at room temperature, was cooled down to 2 K in a SQUID magnetometer. Figure 5 (bottom) shows the magnetization changes for the thus-prepared *cis* film resulting from alternate illumination with visible and UV light at 2 K. During the visible light illumination, the magnetization value increased. Even after the illumination was stopped, this increased magnetization was maintained for at least 2 h. Then, we illuminated the sample with the UV light for a further 10 min. The magnetization value decreased ca. 60%. This value in the changes of the magnetization is consistent with that of the UV–vis spectral change. After that, the visible light-induced increase and UV light-induced decrease of the magnetization were repeated several times. Extended illumination with visible light or UV light did not produce further changes in the magnetization, i.e., the photoinduced magnetization changes saturated after a 10-min illumination. These magnetization changes are consistent with the UV–visible absorption spectral changes and can be explained in the same fashion.

When the film was prepared without washing during the stepwise synthesis process, bulk Prussian blue was formed outside the vesicles, and photo-illumination produced only very small changes (≈0.2%) in the total magnetization. This result suggests that the photo-illumination affects only the Prussian blue intercalated inside the vesicles. On the basis of the above

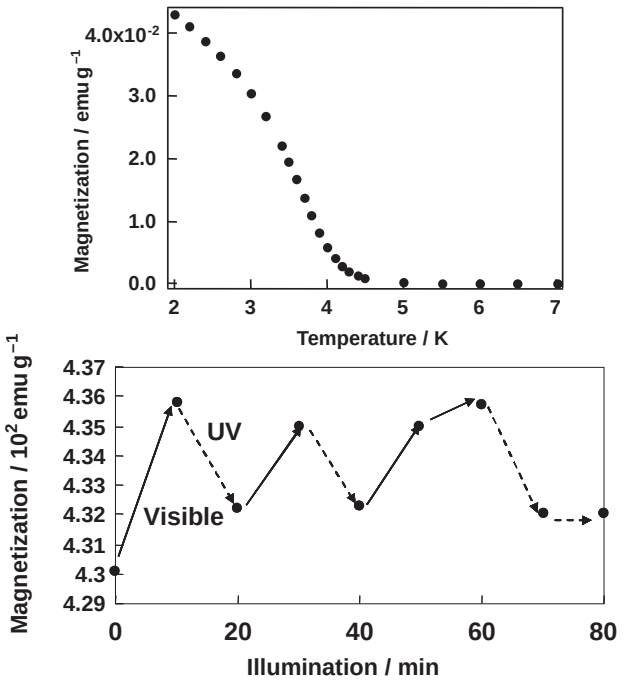

Fig. 5. (top) Field-cooled magnetization curve with an external magnetic field of 5 G at 2 K for *cis* form of the film. This film exhibits ferromagnetic properties with a critical temperature of $T_c = 4.2$ K. (bottom) Changes in the magnetization for the film induced by visible and UV light illumination at 2 K with an external magnetic field of 5 G.

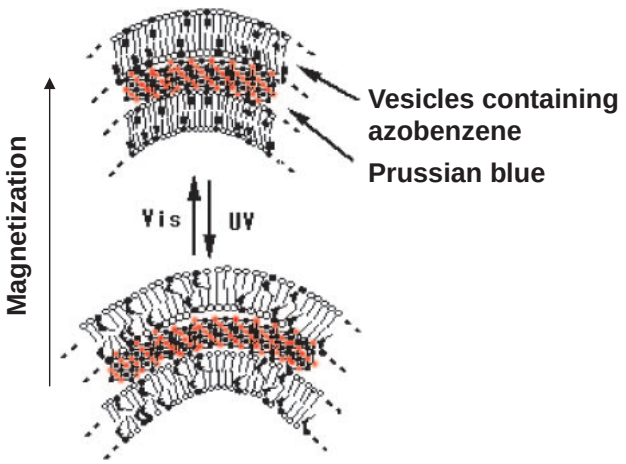

Fig. 6. Schematic illustration of the geometrically confined structural transformations induced by photo-illumination.

results, we have concluded that the magnetization control by light illumination is due to the photo-isomerization of azo moiety in the bilayer membrane. Turbidity (optical absorbance of the film at 662 nm) measurements also indicated that the photo-isomerization of the azo moiety in film induced the changes in the vesicle structure.

Figure 6 shows a schematic illustration of the structural change. It is proposed that photo-isomerization of the film is accompanied by a geometrically confined structural change, as reflected by changes in dipole moment and electrostatic field. Therefore, the magnetization values could be switched reversibly with successive UV and visible light illumination.

In summary, we have designed a first photo-functional composite material comprising Prussian blue intercalated into photo-responsive vesicles whose magnetic properties can be controlled by photo-illumination. Our results suggest that this phenomenon is due to changes in the vesicle structure induced by the photo-isomerization of azobenzene. We believe that this small structural change affects the electrostatic interactions between the Prussian blue and the vesicle bilayer. This work offers new perspectives into photo-functional materials derived from the combination of a functional bilayer assembly and a molecule-based magnetic material.

However, the above system has disadvantages. One of them is that photo-switching degree was very small (ca. 1%). Another point is that the photo-switching phenomena were achieved only at very low temperature (2 K). Therefore, we have designed several new systems to overcome these disadvantages. The designed systems will be described below.

At first, photoswitchable magnetic LB films with well-organized nanoscale layered structure, which were designed in order to enhance the degree of photo-control over the magnetization, are introduced in Section **2**.

2. Photoswitchable Magnetic Films: Prussian Blue Intercalated in Langmuir–Blodgett Films Consisting of an Amphiphilic Azobenzene and a Clay Mineral[21] —Trial for Photo-Switching with High Efficiency—

The photo-controllable magnetic thin film consisting of amphiphilic azobenzene cations, a smectite clay, and Prussian blue has been designed and prepared by using the Langmuir–Blodgett method and an ion-exchange reaction. Here, we have focused on the use of a clay mineral as the template of the composite materials because of several advantages. One of them is the stability of the films with highly ordered structure due to the rigid clay layers. Moreover, it is possible to intercalate some compounds into the films by an ion-exchange reaction with clay layers.

The hybrid multilayered film was composed of an azobenzene derivative {5-[4-(4-dodecyloxyphenylazo)phenoxy]pentyl}-(2-hydroxyethyl)dimethylammonium bromide (=$C_{12}AzoC_5N^+Br^-$) as the amphiphilic cation, montmorillonite (Kunipia P) as the clay mineral, and Prussian blue as the magnetic material (Fig. 7). A schematic illustration of the film preparation process is shown in Fig. 8. The solution of $[C_{12}AzoC_5N]^+Br^-$ was spread on a sub-phase of the clay suspension at room temperature. A floating monolayer of $C_{12}AzoC_5N^+$ was hybridized with the clay platelets at the air–suspension interface. After that, the floating hybrid monolayers were compressed with a surface pressure of 30 mN m^{-1}. After thirty minutes, the floating hybrid monolayers were transferred as X-type films onto the hydrophobic surface of the glass substrates by a horizontal dipping technique. The surface of the transferred film was rinsed with pure water several times, and was then immersed in an aqueous $FeCl_2$ solution to exchange the Fe^{II} ions with the exchangeable metal ions. After rinsing the surface was rinsed well with pure water, it was dipped in an aqueous $K_3[Fe(CN)_6]$ solution to form a Prussian blue layer on the surface of the hybrid film. The hybrid multilayered films were fabricated by repeating this method. One unit layer composed of $C_{12}AzoC_5N^+$, the clay platelets, and Prussian blue is hereafter designated as

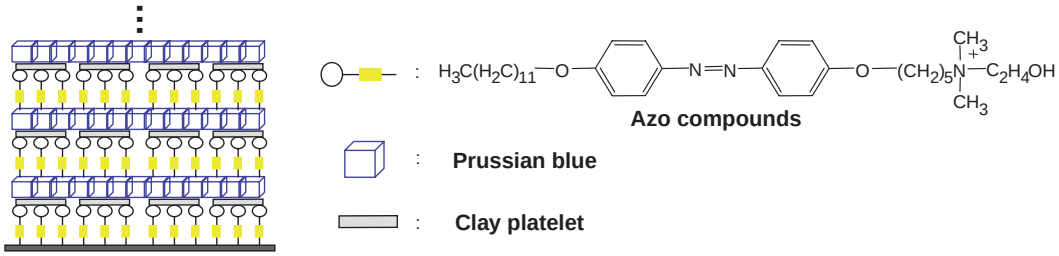

Fig. 7. Design of photo-responsive magnetic thin films containing clay platelets, Prussina blue, and azo compounds.

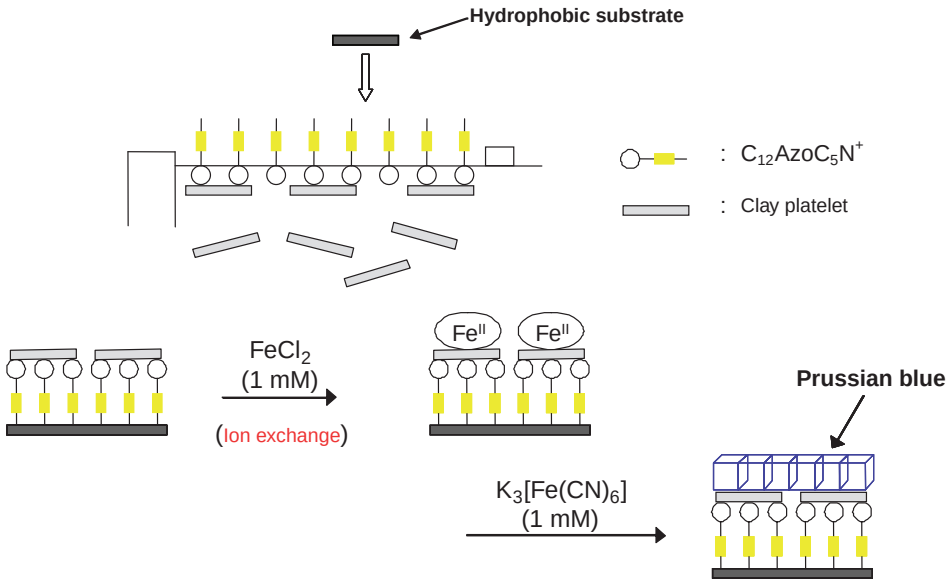

Fig. 8. Preparation of the hybrid multilayered films.

one hybrid layer.

UV–vis absorption spectra of the hybrid multilayered films gave two intense absorption peaks at 370 nm and around 700 nm. The peak at 370 nm is ascribed to the π–π^* transition of the *trans* isomer of $C_{12}AzoC_5N^+$ and the peak at around 700 nm is related to the intervalence charge-transfer (IVCT) band from Fe^{II} to Fe^{III} in the Prussian blue layer. The absorbance increased linearly as the number of hybrid layers increased. This indicates a reproducible transfer of the floating hybrid monolayers from one to the next.

Next, photo-isomerization of the hybrid multilayered films was monitored by UV–vis absorption spectroscopy. The UV–vis spectral changes due to photo-isomerization between *trans* and *cis* state were observed both at room temperature and at 10 K. The XRD pattern indicates that the hybrid film possesses a layered structure. In addition, the thickness of one hybrid layer ($C_{12}AzoC_5N^+$/clay/Prussian blue) is calculated to be 3.27 nm. Considering that the thickness of a clay platelet is 0.96 nm,[22] the total thickness of the $C_{12}AzoC_5N^+$ and Prussian blue layers should therefore be 2.31 nm. Because the layer thickness of $C_{12}AzoC_5N^+$ is estimated to be 1.71 nm, the thickness of the adsorbed Prussian blue layers (–CN–Fe^{III}–NC–Fe^{II}–O) is determined to be 0.60 nm. On this occasion, we suggest that roughly one layer of the three-dimensional Prussian blue network is formed, even in the hybrid multilayered films.

The field-cooled magnetization curve at an external magnetic field of 10 G for the hybrid multilayered films exhibits ferromagnetic properties with a critical temperature (T_c) of 3.2 K. In addition, the presence of a ferromagnetic interaction at low temperature was supported by the plot of the magnetization as a function of an external magnetic field at 2 K, where a magnetic hysteresis loop was observed (Fig. 9 (top)). Subsequently, we observed the influence of light illumination on the magnetic properties of the hybrid multilayered films and also determined how the magnetization changed by alternate illumination with UV and visible light at 2 K (Fig. 9 (bottom)). During the UV light illumination, the magnetization value decreased. Even after the light illumination was stopped, this decreased magnetization value was maintained. Then, after we illuminated the films with visible light, the magnetization value recovered by ca. 55%. After this process, the UV light-induced decrease and the visible light-induced increase of the magnetization were repeated several times. The total photoinduced changes in the magnetization values are estimated to be ca. 11%. By analogy with our previous system,[17] it is proposed that the photo-isomerization of the azobenzene chromophore was accompanied by a geometrically confined structural change, as reflected by changes in the dipole moment and the electrostatic field. Also, in this system, changes in the electrostatic field driven by the photo-isomerization of the azobenzene chromophore led to changes in the Coulombic energy. Such changes are necessary to transfer an electron from the hexacyanoferrate(II) ion to Fe^{III} species, and this might affect the superexchange interaction between the spins in the Prussian blue magnet.

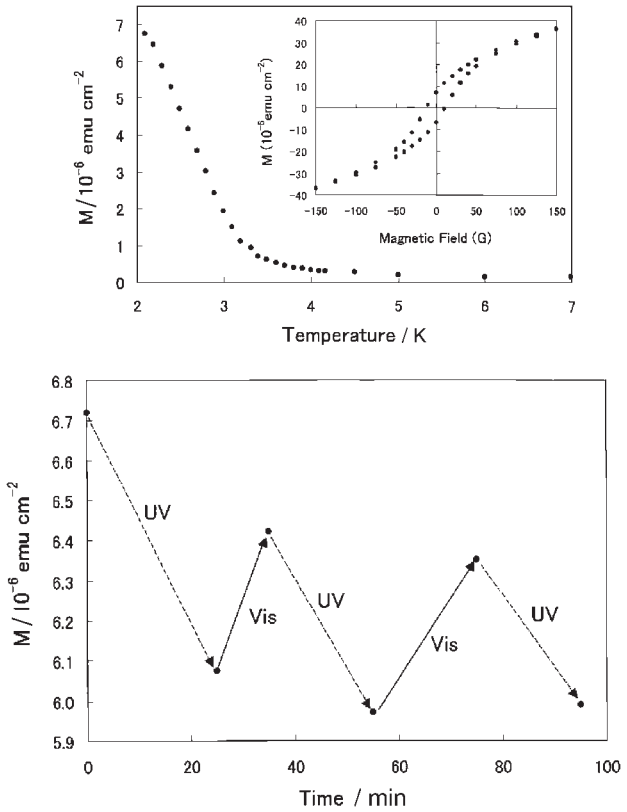

Fig. 9. (top) Field-cooled magnetization curve with an external magnetic field of 10 G for a 24-layered hybrid film. This film exhibits ferromagnetic properties with a critical temperature of $T_c = 3.2$ K. The inset shows hysteresis loop for a 24-layered hybrid film at 2 K. (bottom) Changes in the magnetization for a 24-layered hybrid film, induced by UV and visible light illumination at 2 K with an external magnetic field of 10 G.

We have thus succeeded in designing a photo-functional LB thin film system whose magnetic properties can be controlled by photo-illumination with higher efficiency. This larger photo-switching of the magnetization was due to the formation of well-organized hybrid multilayered films.

Next, trials for photo-control of magnetization at room temperature, are introduced in the next Section.

3. Spiropyran Vesicles Containing Iron Oxide Particles[23] —Magnetization Increase by Photo-Illumination at Room Temperature—

Here, we have focused on the iron oxide particles as magnetic materials at room temperature. Moreover, we have focused on the photoinduced aggregation of spiropyran compound (SP1822).

A commercially available dye SP1822 (8-docosanoyloxymethyl-3′,3′-dimethyl-6-nitro-1′-octadecylspiro[2*H*-chromene-2,2′-indoline]) was purchased. Iron oxide (Fe_3O_4) particles were synthesized according to the literature.[24] The sonicated SP1822 and the iron oxide particles were prepared in deionized H_2O, and the dispersion was mixed with an aqueous solution of poly(vinyl alcohol). The composite film was prepared by casting the above solution onto a clean glass plate at room temperature (Fig. 10).

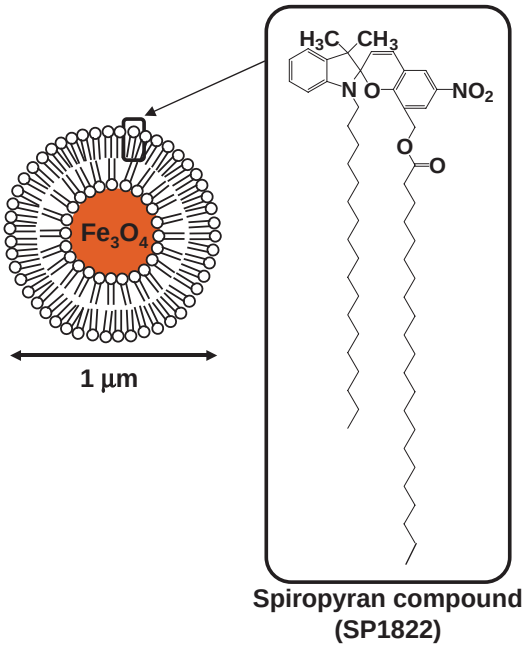

Fig. 10. Design of photo-responsive magnetic vesicles containing iron oxide and spiropyran compounds.

Photoinduced isomerization and aggregation of the vesicles in film was observed by UV–vis absorption spectroscopy (Fig. 11). The film was almost transparent before illumination (absorption band of SP1822 was observed at ca. 240, 270, and 340 nm). In the initial regime of the UV light illumination, the main photoreaction is the isomerization of SP1822 to photo merocyanine isomer (PMC). This reaction meant the decrease in intensities of the absorption bands at ca. 240 and 270 nm as well as the concomitant increase in intensities of the bands at ca. 380 and 560 nm. On prolonged UV light illumination, the formation of a J-aggregation was proposed by the presence of a shoulder band at ca. 620 nm. Normally, the aggregation could only be observed in the special environments such as in Langmuir–Blodgett films of an amphiphilic spiropyran,[25] bilayer membrane,[26] or liquid crystal matrice.[27] In this system, however, the photoinduced aggregation of the vesicles, resulting from the presence of iron oxide particles, was observed even in PVA matrix. Hence, irregular-shaped structures played a significant role in the initial formation and growth of aggregation. The scanning electron micrograph (SEM) image of the films before illumination indicated the presence of the ring-like and spheroidal vesicles with heterogeneous diameters (500–1000 nm). On the other hand, some aggregated objects with cylindrical structure were observed after UV light illumination at room temperature (Fig. 11).

Next, the magnetic properties of the film were studied by SQUID measurements. A typical characteristic of superparamagnetic behavior, showing almost immeasurable coercivity and remanence, was observed at room temperature (Fig. 12 (inset)). The influences of UV light illumination on the magnetic properties of the film at room temperature were observed. During the period of UV light illumination, the magnetization value at 10 G increased (Fig. 12).

In order to study the magnetic dipolar interactions among iron oxide particles before and after UV light illumination,

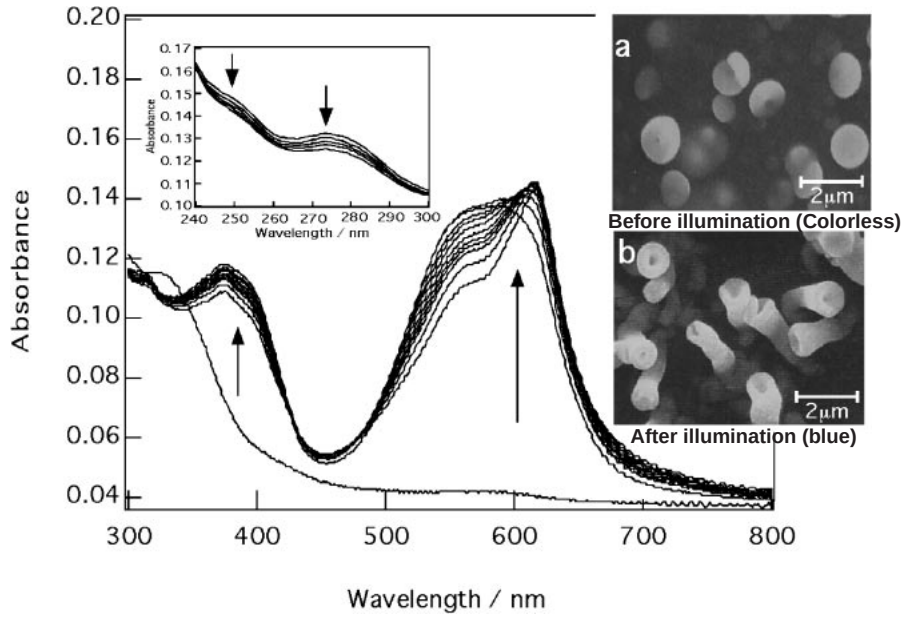

Fig. 11. UV–visible spectral changes of the vesicles on illumination with UV light. The spectra were recorded during the illumination from $t = 0$ min to $t = 180$ min. The inset (left) represents the magnification for short wavelength region. The inset (right) is SEM images of the vesicles (a) before illumination and (b) after 180 min UV light illumination.

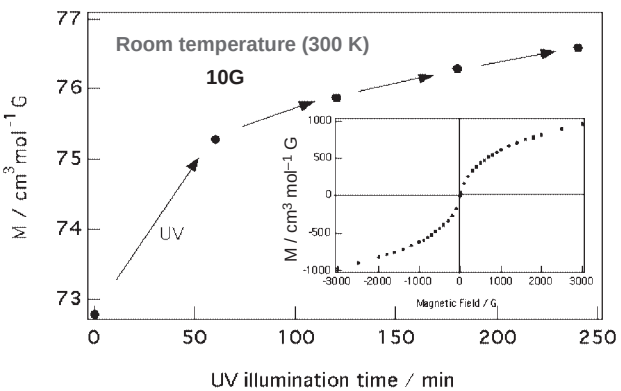

Fig. 12. Changes in the magnetization for the vesicles induced by UV light illumination at 300 K with an external magnetic field of 10 G. During each step, the illumination was continued for 60 min. The inset is magnetization vs applied magnetic field at 300 K for the vesicles.

we also conducted zero-field-cooled (ZFC) susceptibility measurements. Strong inter-particle interaction such as aggregation, as was realized, would result in the increase of the blocking temperature (T_B). The general trend of the change is that T_B shifted towards higher temperature when the interactions between particles increased.

In summary, we have succeeded in increasing the magnetization value of magnetic vesicles of spiropyran containing iron oxide particles by photo-illumination. Although we were able to increase their magnetization values by carrying out photo-illumination at room temperature, the reversible photo-switching of their magnetic properties that we achieved was far below our expectations. This was because the photoinduced increase in the magnetization was due to the aggregation of the iron oxide particles, and we can easily guess that it is difficult for aggregated particles to be separated.

Therefore, next, we have tried to prepare new types of magnets in which the magnetic properties can be controlled reversibly by photo-illumination at room temperature. These efforts are introduced in Section **4**.

4. Reversible Photo-Switching of the Magnetization at Room Temperature[28]

In order to realize the photo-switching reversibly at room temperature, we have focused on a surface modification of nano-scale iron oxide particles and a combination of azobenzene-containing amphiphilic compounds and γ-Fe_2O_3 magnetic nanoparticles as magnetic materials that can function at room temperature. The surface modification of nanoparticles is a useful technique for functionalizing the material properties.[29]

We first designed and synthesized an appropriate azobenzene derivative (Azo) in order to achieve the preparation of our target materials (photo-responsive nano-magnetic materials). An additional strategy that we employed for realizing reversible photo-isomerization (even in the solid state) was not only to encapsulate the surfaces of the γ-Fe_2O_3 nanoparticles with an azo-moiety (Azo), but also to add octylamine, which can supply a free volume in which the azo-moiety can photo-isomerize (Fig. 13).

An amphiphilic azo compound 8-[4-(4-butoxyphenylazo)-phenoxy]octan-1-ol (Azo) and the γ-Fe_2O_3 nanoparticles were first synthesized according to the literature. Then, $FeCl_3 \cdot 6H_2O$, sodium acetate (as a hydrolyzing agent), H_2O, octylamine, and Azo in 1,2-propanediol were heated under reflux. A final solution of the composite materials was then cast onto the substrate for further study.

A transmission electron microscope (TEM) image of the materials indicates the global presence of γ-Fe_2O_3 nanoparticles with almost homogeneous diameters (5 nm) (Fig. 13). The photo-isomerization of the materials on the quartz substrates was monitored by UV–vis absorption spectroscopy at room

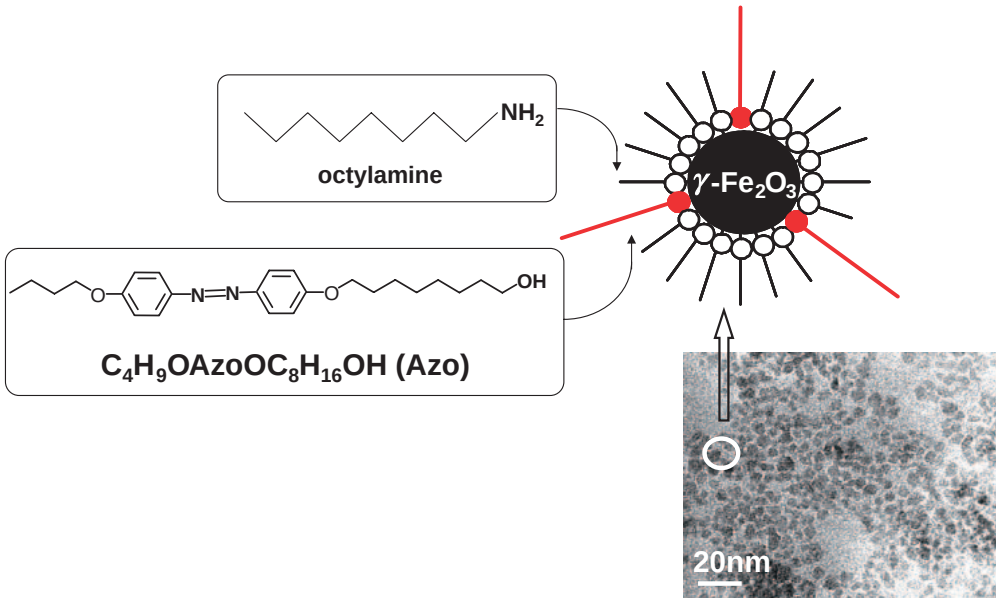

Fig. 13. Design of reversible photo-switching iron oxide nanoparticles coated by azo compounds.

temperature (Fig. 14a). Before illumination, the spectra exhibited two absorption peaks at about 360 nm and a weak band at about 480 nm, which are related to the π–π^* and the n–π^* transition bands of the azo compound with the *trans*-form, respectively. After UV illumination, the intensity of the π–π^* transition band at 360 nm decreased and the intensity of the n–π^* transition band at 480 nm increased, indicating the occurrence of *trans*-to-*cis* photo-isomerization (Figs. 14a(a) and 14a(b)). Following a subsequent illumination with visible light, the reverse process, i.e., the *cis*-to-*trans* isomerization, proceeded to completion (Figs. 14a(a)–14a(c)). The *trans*-to-*cis* photo-isomerization cycles were subsequently repeated several times by alternately illuminating with UV and with visible light. The changes in the absorbance at 360 nm (π–π^* transition bands of the azo compound with the *trans*-form) are shown in Fig. 14b. Because the photo-isomerization of azobenzene derivatives (particularly the *trans*-to-*cis* isomerization reaction) is normally accompanied by an increase in molecular volume, the solid-state reaction is greatly inhibited due to the close packing of the chromophores. In practical terms, when the solid state consists only of Azo, it does not exhibit any photo-isomerization behavior. For the present composite nanoparticles, sufficient free volume is guaranteed in order to allow photo-isomerization by the dilution of the azo moiety with octylamine. Another important strategy for preparing the materials concerns the Lewis basicity of the system. Octylamine, which functions as an encapsulating agent for γ-Fe_2O_3 nanoparticles,[30] contains amino groups, while Azo contains hydroxy groups. This means that Azo takes precedence over octylamine, resulting in the successful preparation of the composite nanoparticles.

The magnetic properties of the materials on a glass substrate were studied by SQUID measurements. The temperature dependence of the magnetization exhibits a cusp around 12 K in the zero-field-cooled (ZFC) susceptibility, and a blocking temperature T_B determined from the branching of the ZFC and field-cooled (FC) data (Fig. 15), showing that the composite nanoparticles exhibited superparamagnetic behavior. The ^{57}Fe Mössbauer spectra for the composite materials at both room temperature and at 8 K also revealed the presence of

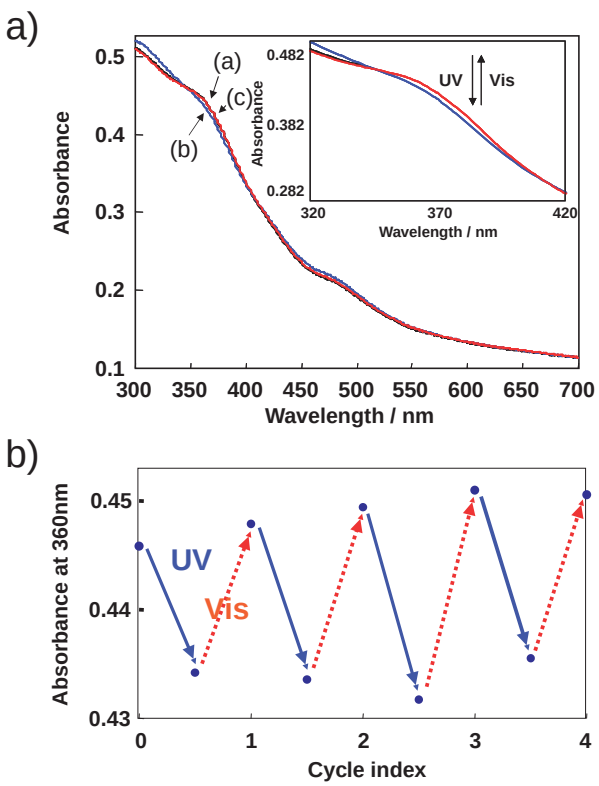

Fig. 14. a) Changes in the optical absorption spectra due to photo-isomerization for the designed nanoparticles cast on quartz substrates at room temperature. (a) Before illumination, (b) after UV light illumination, and (c) after subsequent visible light illumination. b) Changes in absorbance at 360 nm by alternate illumination with UV and visible light.

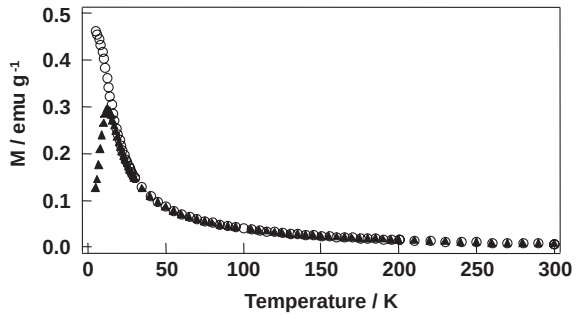

Fig. 15. Magnetization versus temperature at 5 G. (a: ▲) Zero-field cooled (ZFC), (b: ○) field cooled (FC).

γ-Fe_2O_3 nanoparticles. Based on these data, the composite nanoparticles exhibited typical superparamagnetic behavior of magnetic particles, with a particle size that was consistent with that observed by TEM (5 nm).

The magnetization curve at 5 K showed a small hysteresis loop with remanence (5.67 emu g^{-1}) and coercivity (300 G) (Fig. 16a). That is, below the blocking temperature (T_B), the superparamagnetic transition is blocked, i.e., the magnetization cannot relax during the time-frame of the measurement and therefore cannot appear on the plot of magnetization as a function of the magnetic field.

Next, the influence of photo-illumination on the magnetic properties of the composite nanoparticles at 5 K was observed (Fig. 16b). The initial magnetization value of the composite nanoparticles at 10 G increased from 0.279 to 0.305 emu g^{-1} upon UV light illumination. Even after the illumination was stopped, this increased magnetization was maintained for several hours. Then, the nanoparticles were illuminated with visible light for a further 10 min. The magnetization value decreased from 0.305 to 0.280 emu g^{-1}. This UV light-induced increase and visible light-induced decrease in the level of magnetization was repeated several times. The total change induced by photoinduced switching of the magnetization value was ca. 9.3%, which is larger than that achieved by our first photo-functional magnetic vesicle system.[17]

In order to realize devices for practical applications, we performed similar measurements to these at room temperature (300 K). No saturation of the magnetization was found at 300 K with a field of 50000 G. Characteristics that are typical of superparamagnetic behavior were observed, in that almost immeasurable coercivity and remanence were observed (Fig. 17a). This was consistent with the notion that, above T_B, the magnetization should be free to align with the field during the measurement time.

Next, the influence of photo-illumination on the magnetic properties at 300 K was observed. The same tendency for changes in magnetization by photo-illumination were noted i.e. the magnetization value was increased by the use of UV light illumination and decreased by visible light illumination (Fig. 17b). The changes in the magnetization values do not give rise to a distinct trace because of the superparamagnetic properties. These magnetization changes are consistent with the UV–vis absorption spectral changes and can be explained in the same fashion. The reversible control of the magnetic properties of the composite nanoparticles at room temperature was also confirmed by both ESR spectra and ^{57}Fe Mössbauer spectra.

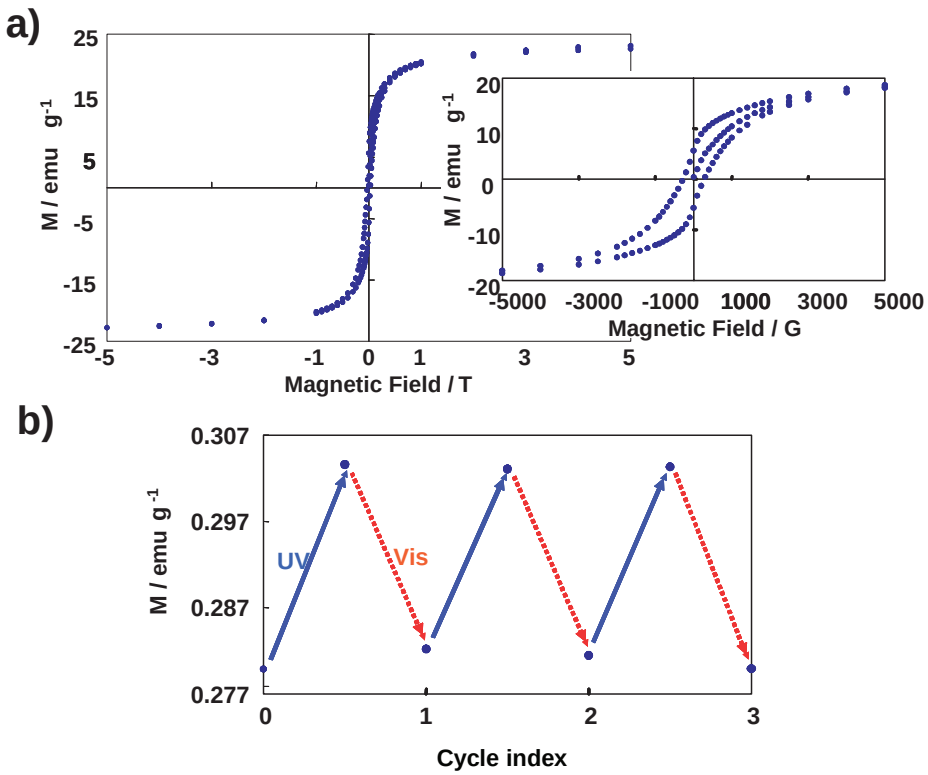

Fig. 16. a) Magnetization versus applied magnetic field at 5 K. The inset shows the magnification. b) Change in the magnetization induced by alternate UV and visible light illumination at 5 K with an external magnetic field of 10 G.

It is suggested that photoinduced changes in the electrostatic field around the γ-Fe_2O_3 magnetic nanoparticles affected the magnetization (Fig. 18). Examples from our previous work could also be explained by similar interactions.[17] Changes in the dipole moments caused by the photo-isomerization of the Azo induced magnetic fields and moments in the materials. First of all, it has been known from our previous results that the changes in the dipole moments of the azo compounds did not affect the magnetization value in the paramagnetic region.[17] Those results were consistent with the present results of the temperature dependence (at 5 K and room temperature). That is, the stronger the magnetic exchange interactions between spins are, the greater effect the dipole moment has on the magnetization values.

The relationship between the electronic polarization (including the charge or the dipole moments) and the magnetization has been discussed previously by several physicists.[31,32] The origins of the magneto-electric behavior of magneto-electric materials are the electric-field-induced *g* shift, spin–orbit interactions, exchange energies, and the electric-field-induced shifts in the single-ion anisotropy energy. The underlying electrodynamics are complicated by induced fields interacting with electric and magnetic moments. That is, the spin orientation is coupled to the electric multi-pole through the lattice. Morup et al. also discussed the existence of significant collective effects in a magnetic nanoparticle system and offered several speculations regarding a spin-glass-like phase at low temperatures on dipole–dipole interacting systems.[32b] Moreover, the surface magnetic phase diagram of the tetragonal manganites depends on the electrostatic interactions caused by the surface environment, such as surface termination.[33]

In 1999, Alivisatos et al. described the preparations of soluble crystalline γ-Fe_2O_3 nanoparticles by high-temperature organic-phase decomposition of an iron precursor.[34] After this report, the process was extended to the synthesis of monodisperse MFe_2O_4 (M = Fe, Co, and Mn) nanoparticles by Sun et al.[35] They used oleic acid and oleylamine for the formation of the particles. They studied the stability of the nanoparticles

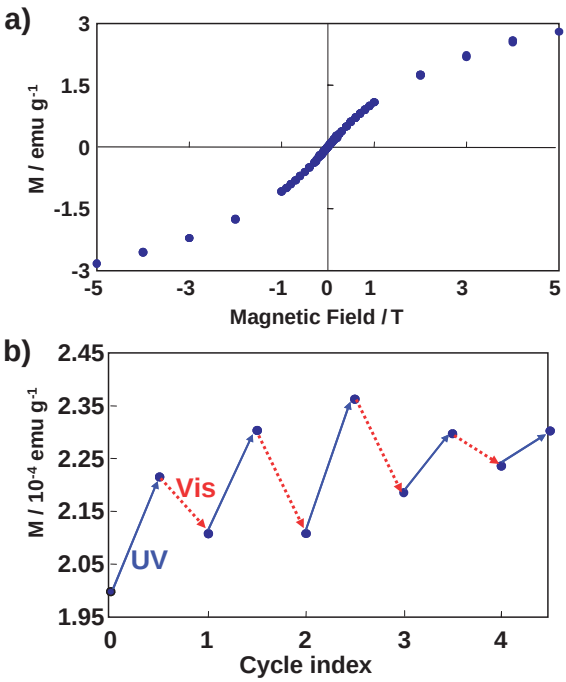

Fig. 17. a) Magnetization versus applied magnetic field at 300 K. b) Change in the magnetization induced by alternate UV and visible light illumination at 300 K with an external magnetic field of 10 G.

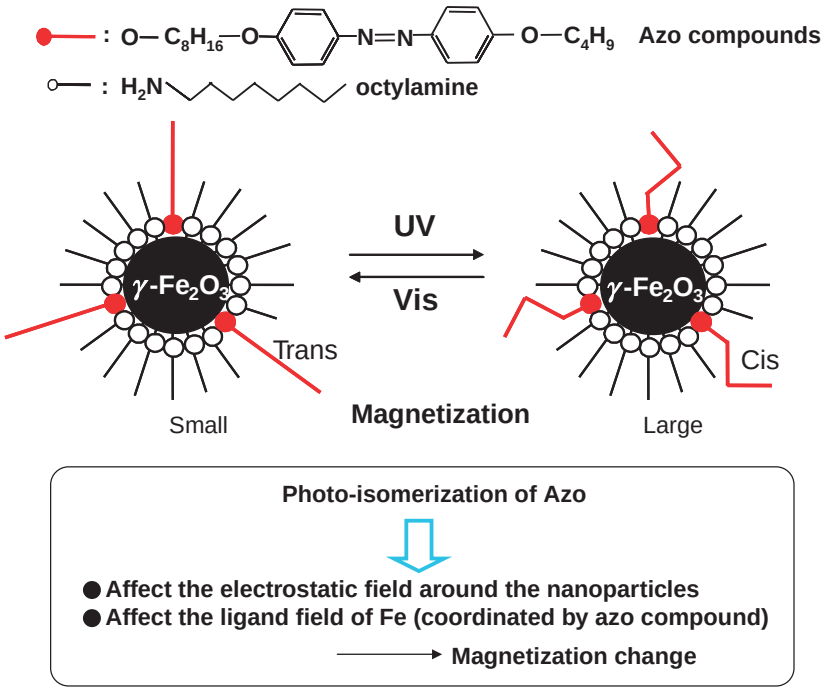

Fig. 18. Mechanisms for the photo-switching of the magnetization.

by varying the ratio of the capping agents and described how γ-Fe_2O_3 nanoparticles can be stabilized by alkylamine surfactants,[29b,30] suggesting that $-NH_2$ coordinates with Fe^{III} on the surface of the particles. Furthermore, Zhang et al. studied the effects of surface coordination chemistry on the magnetic properties of $MnFe_2O_4$ nanoparticles.[36a,b] They observed that the coercivity of magnetic nanoparticles decreased upon coordination of the ligands on the nanoparticle surface, whereas the saturation magnetization increased. They concluded that the change in magnetic properties of the nanoparticles correlates with the specific coordinating functional group bound onto the nanoparticle surface and that the correlations suggest a decrease in the spin–orbital coupling and surface anisotropy of magnetic nanoparticles due to surface coordination. Furthermore, Gedanken et al. also studied the magnetic properties, especially the blocking temperature T_B, of iron nanoparticles coated by various surfactants.[36c] They observed large variations in the blocking temperature for various functional groups bonded to the iron nanoparticles. For example, the magnetization values for alcohols and carboxylic acids were different from those for sulfonic and phosphonic acid. They also discussed why these differences could be explained not only by variations of particle size, but also through the effects of the functional group bonded to an iron atom on the d electrons of the iron. The functional groups interact strongly with the d electrons and cause a large splitting of the doubly- and triply-degenerate d levels. This affects the spin state and the magnetization values. Thus, this suggests that exchange interactions between the spins of the iron affect the magnetization.

The above discussions also suggest that photoinduced changes in the electrostatic field around the γ-Fe_2O_3 magnetic nanoparticles affect the magnetization. Photo-switchable magnetic films (Prussian blue intercalated in Langmuir–Blodgett films consisting of an amphiphilic azobenzene and a clay mineral),[21] which was introduced in Section **2**, supplied data that supports these mechanisms. An intervalence charge-transfer (IVCT) band between Fe^{II} to Fe^{III} in the Prussian blue layer was changed reversibly by alternate UV and visible light illumination accompanied by photo-isomerization of the azo compound. That is, changes in the electrostatic field driven by the photo-isomerization of the azobenzene chromophore led to changes in the Coulombic energy (which is necessary to transfer an electron) and this might affect the superexchange interaction between the spins in the Prussian blue magnet.

In summary, we have designed novel photo-responsive γ-Fe_2O_3 nanoparticles that are encapsulated by an azo compound and octylamine. To photo-control the magnetization, the design of the interfaces between the photo-responsive materials and the magnetic materials is important. The advantage of this system was that nano-scale particles from which much larger areas of photo-responsive interfaces might be expected, were used as the magnetic materials. Another important aspect was the dilution of the azo moiety with *n*-octylamine. The free volume gained is responsible for the ideal photoreaction. Use of azo compounds with appropriate end-groups and alkyl chain lengths for direct interaction with the metal oxide surface was also important. Finally, we have succeeded in switching the magnetization value of composite magnetic nanoparticles by photo-illumination *in the solid state at room temperature*.

Conclusion

Several interesting photo-switching magnetic systems using similar strategy have been reported. Yu et al. reported a photochromic molecule-based magnetic materials with alternating ferromagnetic layer $[MnCr(ox)_3]_n^{n-}$ and cationic spiropyran layer.[37,38] UV light illumination transformed the initially very soft magnet into a much harder one, as evidenced by the dramatic and irreversible changes in the shape of hysteresis loop, although the change is irreversible. A spectacular change in the hysteresis loop was ascribed to photoinduced defects in the crystal structure through the photoreaction of a spiropyran derivative. They also reported another similar work in intercalating cationic spiropyrans into regid layered $MnPS_3$ materials, where a reversible photo-switching of magnetic coercivity.[39] Kojima et al. also reported a reversible photomagnetism in a cobalt layered compound coupled with photochromic diarylethene ($Co_4(OH)_7$[anionic diarylethene])$_{0.5}\cdot 3H_2O$).[40] We also fabricated a photo-switchable magnetic layer-by-layer thin films consisting of azobenzene and iron oxide nanoparticles, which could be prepared with very simple technique.[41] It is thus important to note that, recently, several scientists are also trying to prepare novel photomagnetic materials by using this strategy, i.e., photochromic organic and inorganic magnetic systems.

The present work will yield much valuable information, not only bringing new perspectives into photo-functional materials derived from a combination of photo-functional organic materials and inorganic magnetic materials, but also leading to future applications of nanomagnetic materials, which are currently attracting growing interest in ultrahigh-density magnetic recording systems.

The author would like to express thanks to Prof. Osamu Sato (Kyushu University) for giving me valuable suggestions. I also wish to express my thanks to my supervisor, Prof. Akira Fujishima (KAST) and Prof. Kazuhito Hashimoto (The University of Tokyo) for superb guidance in this work. Finally, I would like to express my thanks to all of co-workers, especially graduate students in our group, Mr. Taguchi, Mr. Yamamoto, and Ms. Mikami (Keio University). This work was partly supported by Grant-in-Aid for Scientific Research on Priority Areas (417) and the 21st Century COE program "KEIO Life Conjugate Chemistry" from the Ministry of Education, Culture, Sports, Science and Technology (MEXT) of the Japanese Government.

References

1 W. Kuch, *Nature Mater.* **2003**, *2*, 505.

2 C. Thirion, W. Wernsdorfer, D. Mailly, *Nature Mater.* **2003**, *2*, 524.

3 P. Gütlich, Y. Garcia, T. Woike, *Coord. Chem. Rev.* **2001**, *219–221*, 839.

4 a) O. Sato, *J. Photochem. Photobiol., C* **2004**, *5*, 203. b) O. Sato, S. Hayami, Y. Einaga, Z. Gu, *Bull. Chem. Soc. Jpn.* **2003**, *76*, 443.

5 A. Bousseksou, G. Molnar, G. Matouzenko, *Eur. J. Inorg. Chem.* **2004**, 4353.

6 O. Sato, T. Iyoda, A. Fujishima, K. Hashimoto, *Science*

1996, *272*, 704.
7 Y. Arimoto, S. Ohkoshi, Z. J. Zhang, H. Seino, Y. Mizobe, K. Hashimoto, *J. Am. Chem. Soc.* **2003**, *125*, 9240.
8 G. Li, T. Akitsu, O. Sato, Y. Einaga, *J. Am. Chem. Soc.* **2003**, *125*, 12396.
9 S. Hayami, Z. Gu, M. Shiro, Y. Einaga, A. Fujishima, O. Sato, *J. Am. Chem. Soc.* **2000**, *122*, 7126.
10 S. Mann, J. P. Hannington, R. J. P. Williams, *Nature* **1986**, *324*, 565.
11 M. C. Kanatzidis, C.-G. Wu, H. O. Marey, C. R. Kannewurf, *J. Am. Chem. Soc.* **1989**, *111*, 4139.
12 G. A. Ozin, *Adv. Mater.* **1992**, *4*, 612.
13 S. Mann, D. D. Archibald, J. M. Didymus, T. Douglas, B. R. Heywood, F. C. Meldrum, N. J. Reeves, *Science* **1993**, *261*, 1286.
14 B. R. Heywood, S. Mann, *Adv. Mater.* **1994**, *6*, 9.
15 N. Kimizuka, *Adv. Mater.* **2000**, *12*, 1461.
16 K. Kuroiwa, T. Shibata, A. Takada, N. Nemoto, N. Kimizuka, *J. Am. Chem. Soc.* **2004**, *126*, 2016.
17 Y. Einaga, O. Sato, T. Iyoda, A. Fujishima, K. Hashimoto, *J. Am. Chem. Soc.* **1999**, *121*, 3745.
18 K. Itaya, T. Ataka, S. Toshima, *J. Am. Chem. Soc.* **1982**, *104*, 4767.
19 M. B. Robin, *Inorg. Chem.* **1962**, *1*, 337.
20 A. Ito, M. Suenaga, K. Ono, *J. Chem. Phys.* **1968**, *48*, 3597.
21 T. Yamamoto, Y. Umemura, O. Sato, Y. Einaga, *Chem. Mater.* **2004**, *16*, 1195.
22 D. M. Moore, R. C. Reynolds, Jr., *X-ray Diffraction and the Identification and Analysis of Clay Minerals*, Oxford University Press, New York, **1997**.
23 a) Y. Einaga, M. Taguchi, G. Li, T. Akitsu, Z. Gu, T. Sugai, O. Sato, *Chem. Mater.* **2003**, *15*, 8. b) M. Taguchi, G. Li, Z. Gu, O. Sato, Y. Einaga, *Chem. Mater.* **2003**, *15*, 4756.
24 Y. Liu, A. Wang, R. O. Claus, *Appl. Phys. Lett.* **1997**, *71*, 2265.
25 E. Ando, M. Miyazaki, K. Morimoto, H. Nakahara, K. Fukuda, *Thin Solid Films* **1985**, *21*, 133.
26 T. Seki, K. Ichimura, *J. Phys. Chem.* **1990**, *94*, 3769.
27 I. Gabrera, J. Shvartsman, O. Beinberg, V. Krongauz, *Science* **1984**, *26*, 341.
28 R. Mikami, M. Taguchi, K. Yamada, K. Suzuki, O. Sato, Y. Einaga, *Angew. Chem., Int. Ed.* **2004**, *43*, 6135.
29 a) A. Manna, P.-L. Chen, H. Akiyama, T.-X. Wei, K. Tamada, W. Knoll, *Chem. Mater.* **2003**, *15*, 20. b) A. K. Boal, K. Das, M. Gray, V. M. Retello, *Chem. Mater.* **2002**, *14*, 2628. c) S. Thimmaiah, M. Rajamathi, N. Singh, P. Bera, F. Meldrum, N. Chandrasekhar, R. Seshadri, *J. Mater. Chem.* **2001**, *11*, 3215.
30 M. Rajamathi, M. Ghosh, R. Seshadri, *Chem. Commun.* **2002**, 1152.
31 V. K. Sharma, F. Waldner, *J. Appl. Phys.* **1977**, *48*, 4298.
32 a) J. Baker-Jarris, P. Kabos, *Phys. Rev. E* **2001**, *64*, 056127. b) S. Morup, E. Tronc, *Phys. Rev. Lett.* **1994**, *72*, 3278.
33 J. C. Mallinson, *The Foundations of Magnetic Recording*, Academic, Berkeley, **1987**, Chap. 3.
34 J. Rockenberger, E. C. Scher, P. A. Alivisatos, *J. Am. Chem. Soc.* **1999**, *121*, 11595.
35 a) S. Sun, H. Zeng, *J. Am. Chem. Soc.* **2002**, *124*, 8204. b) S. Sun, H. Zeng, D. B. Robinson, S. Raoux, P. M. Rice, S. X. Wang, G. Li, *J. Am. Chem. Soc.* **2004**, *126*, 273.
36 a) C. R. Vestal, Z. J. Zhang, *J. Am. Chem. Soc.* **2003**, *125*, 9828. b) C. Liu, B. Zou, A. J. Rondinone, Z. J. Zhang, *J. Am. Chem. Soc.* **2000**, *122*, 6263. c) G. Kataby, Y. Koltypin, A. Ulman, I. Felner, A. Gedanken, *Appl. Surf. Sci.* **2002**, *201*, 191.
37 S. Benard, E. Riviere, P. Yu, K. Nakatani, F. Delouis, *Chem. Mater.* **2001**, *13*, 159.
38 K. Nakatani, P. Yu, *Adv. Mater.* **2001**, *13*, 1411.
39 S. Benard, A. Leaustic, E. Riviere, P. Yu, R. Clement, *Chem. Mater.* **2001**, *13*, 3709.
40 M. Okubo, M. Enomoto, N. Kojima, *Solid State Commun.* **2005**, *134*, 777.
41 M. Suda, Y. Miyazaki, Y. Hagiwara, O. Sato, S. Shiratori, Y. Einaga, *Chem. Lett.* **2005**, *34*, 1028.

Yasuaki Einaga was born in Niigata, Japan in 1971. He graduated from the Department of Chemistry, The University of Tokyo in 1994, and received M.Sci. (1996). He received his Ph.D. degree in 1999 from Department of Applied Chemistry, The University of Tokyo under the direction of Prof. Akira Fujishima. After a position of Research Associate in Prof. Fujishima's group, he joined the Department of Chemistry at Keio University as an Assistant Professor in 2001. In 2003, he was promoted to Associate Professor. His research interests include photo-functional materials science and diamond electrochemistry.